Modelling of UWB Antenna Perturbed by Human Phantom in Spherical Harmonics Space

Mhedhbi, Meriem; Avrillon, Stephane; Pedersen, Troels; Uguen, Bernard

Published in:
Antennas and Propagation (EuCAP), 2014 8th European Conference on

DOI (link to publication from Publisher):
10.1109/EuCAP.2014.6902600

Publication date:
2014

Document Version
Early version, also known as pre-print

Modelling of UWB Antenna Perturbed by Human Phantom in Spherical Harmonics Space

Meriem Mhedhbi[1], Stéphane Avrillon[1], Troels Pedersen[2], Bernard Uguen[1],
[1] IETR, University of Rennes 1, France, meriem.mhedhbi, stephane.avrillon, bernard.uguen@univ-rennes1.fr
[2] Department of Electronic Systems, Aalborg University, Denmark, troels@es.aau.dk

***Abstract*—In this paper we study how the antenna radiation pattern is perturbed in the presence of a human phantom in terms of changes in the coefficients of the spherical harmonic antenna representation. The spherical harmonic basis allows for a compact representation of the antenna pattern which is attractive for simulation purposes. We propose a simple model for the spherical harmonics coefficients allowing to predict the antenna behavior perturbed by a human phantom. The model is based on knowledge of the spherical harmonic coefficients of antenna in free space and the antenna-phantom distance.**

***Index Terms*—UWB antenna, spherical harmonics, Body Area Networks, antenna measurement.**

I. Introduction

In the context of modelling and simulation of the radio channel experienced in a wireless body area network (WBAN), the knowledge of the antenna radiation pattern is important. Moreover, a nearby body affects the antenna pattern and should therefore be included in the simulation model. However, this poses a number of challenges.

Firstly, if relying directly on measurements of the antenna alone, the obtained radiation pattern should be adapted to include the presence of the human body. For this purpose, simple models describing the relation between simple parameters such as antenna-body distance and body size would be of importance. Secondly, if relying on measurements of the combined of an antenna and body a new data set for each pair of antennas and bodies should be measured. The potential large number of combinations of body parts, distances, and antennas, would require a large database of antenna measurement data, which is inconvenient in such a simulator. It is therefore natural to consider models in which the antenna pattern for each antenna body configuration can be represented by only few coefficients and where the pattern reconstruction is straightforward.

In this work, we approach the antenna data storage problem by means of expansion of the pattern in spherical harmonics (SH) [1], [2], [3]. In the SH basis, the full antenna data can be compressed to only a few coefficients. Traditionally, vector spherical harmonic (VSH) expansion have been the most popular basis for representation of far-field antenna radiation patterns because it preserves inherently the transversal field. While this feature is attractive, the VSH basis has the drawback of more complicated basis functions burdening the reconstruction task. We follow the alternative approach proposed in [4] of expanding the radiation pattern in terms of scalar spherical harmonics (SSHs).

In the present contribution, we study the effect of the human body presence close to the antenna in terms of SSH coefficients variation. In particular, we focus on the change in the expansion coefficients as a function of phantom-antenna distance. We propose and validate a model for the SSH coefficients able to predict the observed variation of antenna radiation pattern.

In this paper, the measurement campaign and the extraction of spherical harmonics coefficients are presented in section II. The section III is dedicated to the data analysis and a presentation of the most important observations which are the key of the model elaboration. In section IV the proposed model structure is presented. Finally, the model results and validation are presented in section V.

II. Measurement and Post-Processing

A. Measurement Setup

For the study, we designed a measurement campaign specifically to study the antenna response variation in the presence of a dielectric cylinder acting as a human phantom for different antenna/phantom distances (d). The antenna radiation pattern was measured in a SATIMO SG32 near-field measurement chamber at IETR. As depicted in Fig. 1, the presence of a human arm was mimicked by a phantom mounted in the vicinity of the antenna using a custom-made platform of dielectric foam with relative permittivity close to unity. The phantom consists of a nearly cylindrical plastic bottle with a radius $35\,\mathrm{mm}$ filled with MSL1800 phantom liquid. The size and shape of the phantom was chosen to represent a human arm, while still being lighted enough for the platform to support it. The bottle was fitted with a screw in the bottom to allow for mounting on the platform groove or holes. We measured the radiation of the two UWB antennas depicted in Fig.2. We use the data obtained for the "Thomson 1 antenna" [5] for model fitting and the data obtained for the "fractal antenna" for model validation. A detailed description of the measurement setup is available in [6].

The obtained data consists of the far-field pattern of the antenna measured at frequencies $f = [0.8, 5.95]$ GHz in steps of 50 MHz for different phantom distances $d = [30, 135]$ mm in steps of 5 mm. Using Cartesian coordinates, we represent the far-field pattern by a three-dimensional complex vector function $\mathbf{F_c}(\theta, \phi, f, d)$ of co-elevation θ, azimuth ϕ, frequency f, and distance d. The antenna pattern is sampled on the

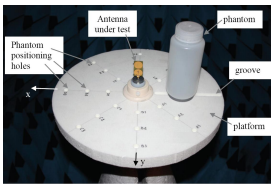

Fig. 1: Measurement Platform

Fig. 2: Thomson 1 (left), fractal structure (right) antennas

sampling grid given by:

$$(\theta_i, \phi_j) = \left(\frac{i}{N_\theta}, \frac{2j}{N_\phi}\right)\pi \tag{1}$$

where $0 \leq i \leq N_\theta$, $0 \leq j < N_\phi$. In the used dataset $N_\theta = 91$ and $N_\phi = 180$. Examples of horizontal cuts of the collected radiation patterns are reported in Fig. 3.

B. Extraction of Scalar Spherical Harmonics Coefficients

Following [4], [7], the far-field radiation pattern is represented in Cartesian systems and expanded in terms of SSHs with vector coefficients:

$$\mathbf{F_c}(\theta, \phi, f, d) = \begin{pmatrix} F^x \\ F^y \\ F^z \end{pmatrix} = \sum_{l=0}^{L} \sum_{m=-l}^{l} \mathbf{c}_{lm}(f, d) Y_l^m(\theta, \phi), \tag{2}$$

where the SSH function of level l and mode m is defined by:

$$Y_l^m(\theta, \phi) = \sqrt{\frac{(2l+1)(l-m)!}{4\pi(l+m)!}} P_l^m(\cos\theta) e^{im\phi} \tag{3}$$

with P_l^m denoting the associated Legendre polynomials of level l and mode m. We limit the expansion to a maximum level denoted by L. The norm $E_{lm} = \|\mathbf{c}_{lm}(f, d)\|^2$ is the energy of mode (l, m). The total energy $E(f, d)$ is the sum of all $E_{lm}(f, d)$ over l, m. The "Mode m energy" E_m and "level l energy" E_l, respectively, are defined as :

$$E_m(f, d) = \sum_{l=|m|}^{L} E_{lm}(f, d)$$

$$E_l(f, d) = \sum_{m=-l}^{l} E_{lm}(f, d)$$

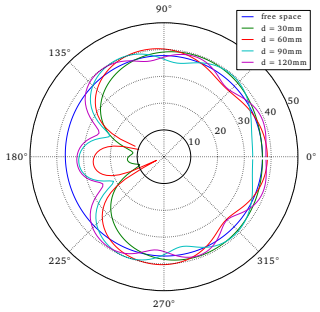

Fig. 3: Magnitude of antenna radiation pattern (dB) at 3.1 GHz for different phantom configurations (x, y) plane.

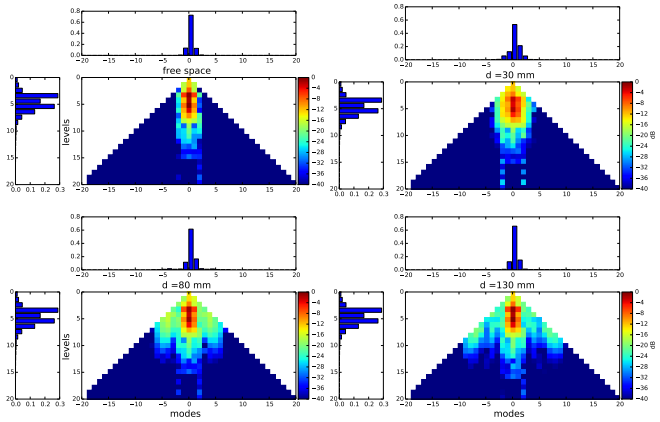

Fig. 4: Magnitude in dB of SSH coefficients ($\|\mathbf{c}_{lm}(f, d)\|$) at $f = 3.1$ GHz with different phantom configurations with relative mode (top) and level (left) energy

The SSH vector coefficients are obtained via least squares for a particular frequency and distance as follows. At each directional grid point, the antenna response for fixed f and d is a three-dimensional complex vector. We arrange these $N_\theta N_\phi$ vectors as columns in the matrix $\mathbf{F_c}(f, d)$ of dimension $(3, N_\theta N_\phi)$. With this definition, the expansion in (2) reads:

$$\mathbf{F_c}(f, d) = \mathbf{C}(f, d)\mathbf{Y} \tag{4}$$

where the entries of the $\left((1+L)^2, N_\theta N_\phi\right)$ matrix $\mathbf{Y}$, are the spherical harmonic functions evaluated at the directional sampling grid. The matrix, $\mathbf{C}(f, d)$ is of dimension $\left(3, (1+L)^2\right)$ with the $\mathbf{c}_{lm}(f, d)$ as columns arranged accordingly. The coefficients $\mathbf{c}_{lm}(f, d)$ are obtained in a straight forward manner by the least squares method as

$$\hat{\mathbf{C}}(f, d) = \mathbf{F_c}(f, d)\mathbf{Y}^+ \tag{5}$$

where $\mathbf{Y}^+$ is the Moore-Penrose pseudo-inverse of $\mathbf{Y}$. Fig. 4 shows examples of SSH coefficients corresponding to the radiations patterns reported in Fig. 3.

III. Observations from Measurements

Based on the data, we have made a number of observations regarding the change in SSH coefficients due to the presence of the phantom. These observations motivate the model structure to be proposed in Sec IV.

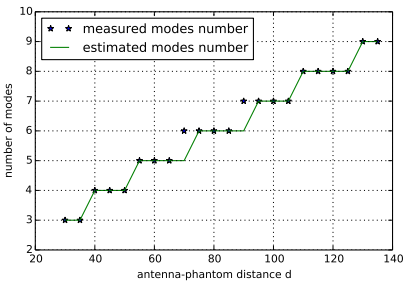

Fig. 5: Number of significant modes M versus distance d with stair-case fitting for $\beta = 0.055$ and $\gamma = 1.0$

A. Observation 1: Number of Significant Modes Versus Distance

The number of significant modes M is the largest integer such that $E_m < 0.01E$ for all $m > M$, i.e. M is the number of modes with energy larger than $1\,\%$ of the total energy E. The coefficients with $m > M$ are considered insignificant. The number of significant modes is a measure for the directivity of the antenna. For omnidirectional antennas, $M = 0$. It appears from Fig. 5 that the number of significant modes as a function of distance is well fitted by a stair-case function

$$M = \lceil \beta d \rceil + \gamma \tag{6}$$

where $\lceil . \rceil$ is the ceiling function. Fig. 3 shows that, as expected, the antenna pattern is radiating mostly in the half space opposite to the phantom and converges to the free space case when d increases. It also appears that at large distances, the antenna pattern ripples around the free space pattern. These ripples might be the origin of the increase of modes number to represent the perturbed antenna shown in Fig. 4. The total energy is split over higher modes while the level energies remain constant.Thus the free space modes energy is distributed over higher modes but the sum is always the same. An alternative interpretation for the observation is related to the fact that the number of coefficient depends on antenna dimensions [7],[8].

B. Observation 2: Omnidirectional mode 0 energy variation

The transition from directive antenna pattern for small phantom-antenna distances to a more omnidirectional for large distances can be observed as a change in the Mode 0 energy reported in Fig. 6.

C. Observation 3: Coefficient Correlation Functions

As appears from Fig.4, the presence of the phantom induces the appearance of new coefficients. To identify a possible correlation between coefficients and to gain insight into the origin of the new coefficients we now consider correlations between the coefficients of the patterns for the free space and the perturbed cases. We aggregate indices l and $m \geq 0$ into one index k according to:

$$\mathbf{c}_k = \mathbf{c}_{lm} \quad , k = \frac{m\,(2L + 1 - m)}{2} + l \tag{7}$$

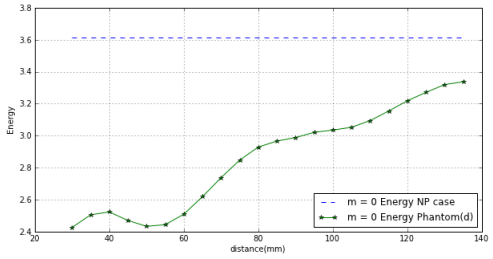

Fig. 6: Mode 0 energy w.r.t antenna/phantom distance

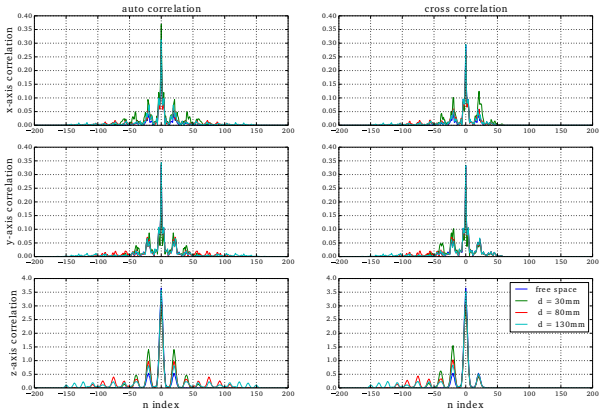

Fig. 7: Auto correlation coefficient (x-axis, y-axis, z-axis) function (left), cross correlation function between coefficient in free space and in phantom presence (right) at $f_0 = 3.1$ GHz. Maximum level is $L = 20$.

Notice that there is a one-to-one correspondence between k and $(l, m \geq 0)$ and thus the index k uniquely identifies an index pair $(l, m \geq 0)$. Regarding indices pairs $(l, m < 0)$ are arranged and stacked using the same way. Thus indices $0 \leq k \leq (1 + L)(2 + L)/2$ correspond to $(l, m \geq 0)$ and $(1 + L)(2 + L)/2 \leq k \leq (1 + L)^2$ are matching $(l, m < 0)$. We now define the cross-correlation function of the free space and perturbed antenna coefficients as:

$$\mathbf{r}\,(n) = \sum_{k=0}^{(1+L)(2+L)/2} \mathbf{c}_k^{fs}\,(f_0)\,\overline{\mathbf{c}_{k+n}\,(f_0, d)} \tag{8}$$

where $\mathbf{c}_k^{fs}\,(f_0)$ are free space antenna coefficients, $\mathbf{c}_{k+n}\,(f_0, d)$ are coefficients with phantom at distance d and the overbar denotes complex conjugate. The auto-correlation of the free space coefficients is obtained by replacing the perturbed pattern in (8) by the free space pattern. To compute the correlation function we use only $\mathbf{c}_k$ because of the relation $\mathbf{c}_{l,-m} = (-1)^m\,\overline{\mathbf{c}_{lm}}$.

Fig. 7 shows that the cross-correlation function exhibits a periodic decaying sidelobes. Furthermore, as the distance increases, the number of sidelobes increases with distance while their height reduce. The free space antenna is represented only by modes $m \in \{0, 1\}$, and the number of peaks in the cross correlation functions exceeds 2. Thus we assume a strong correlation between the new and free space modes (coefficients are arranged by modes), especially that the number of peaks increases with d.

IV. Proposed Model Structure

We now propose a model with low computational complexity for the perturbation of the free space antenna radiation pattern due to the presence of the phantom in terms of the SSH coefficients. The model structure is motivated by the observations presented above.

We first determine the number of significant modes M_{fs} of the free space antenna pattern. Then, the number of significant modes of the perturbed antenna denoted by M_{p} is determined using (6) of *Observation 1*. Motivated by *Observation 2*, we assume that the perturbation for coefficients $m \leq M_{\text{fs}}$ is multiplicative and varies linearly with the distance. Moreover, the coefficients with $M_{\text{fs}} < m < M_{\text{p}}$ which appear due to the phantom is modelled by extrapolating from the free space coefficients. Motivated by *Observation 3* which reveals a strong correlation between the free space $m \leq M_{\text{fs}}$ and the new $M_{\text{fs}} < m < M_{\text{p}}$ modes, the extrapolation is obtained as a scaled copy of mode M_{fs} of the free space antenna. Consequently, we propose to model the perturbed coefficients as

$$\mathbf{c}_{lm}(f,d) = \alpha_m(d)\, e^{j\phi_m(d)} \cdot \begin{cases} \mathbf{c}^{\text{fs}}_{lm}(f), & m \leq M_{\text{fs}} \\ \mathbf{c}^{\text{fs}}_{lM_{\text{fs}}}(f), & M_{\text{fs}} < m \leq M_{\text{p}} \\ 0, & m > M_{\text{p}} \end{cases} \tag{9}$$

where $\{\mathbf{c}^{\text{fs}}_{lm}(f)\}$ denotes the coefficients of the free space antenna pattern. For simplicity, and due to *Observation 2*, we model the real-valued amplitude $\alpha_m(d)$ linearly in d according to

$$\alpha_m(d) = \begin{cases} ad + b, & m \leq M_{\text{fs}} \\ \dfrac{a'd + b'}{m - M_{\text{fs}}}, & M_{\text{fs}} < m \leq M_{\text{p}}. \end{cases} \tag{10}$$

Thus in the model, the amplitude scaling of free space coefficients depend only on d, while the amplitude of new coefficients depend on both m and d.

For $m < M_{\text{fs}}$ we set $\phi_m(d) = 0$ and for $M_{\text{fs}} < m \leq M_{\text{p}}$, $\phi_m(d) = (a''d + b'')m$. Notice that this model replicates the effect which can be seen in Fig. 4, that as d increases the number of significant modes increases at the same time, the amplitude of higher modes decreases.

The proposed model is frequency independent in the sense that only the SSH coefficients of the free-space pattern depends on frequency, *cf.* (9). Furthermore, the model does not depend on the level l because of the particular measurement setup where the phantom is parallel to the z-axis and thus affecting the symmetry over ϕ which in turn affect the modes. The simple linear form of the model brings a low computational complexity as desired.

V. Model Fitting and Validation

A. Model Fitting

We fit the model to the measurements of the Thomson 1 [5] antenna depicted in Fig. 2. Coefficients a, b, a', and b' of be obtained by linear regression of the Mode 0 energy. We find a'' and b'' by linear regression of the phase. The obtained parameter values are collected in Table I.

TABLE I: Fitted Model Parameters

Parameters	a	b	a'	b'	a"	b"
Values	0.002	0.55	-0.002	1.55	-0.006	1.22

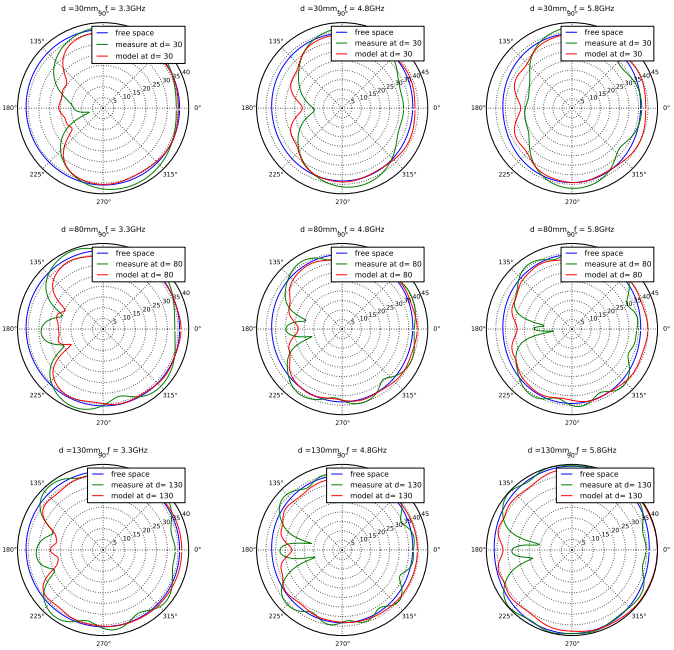

Fig. 8: Comparison of free-space, measured and modelled (fitted) radiation pattern in the (x,y)-plane for the Thomson 1 antenna at different frequencies.

It appears from the sign of the a and a' values in the table that the amplitude $\alpha_m(d)$ exhibit distinct behavior depending on m. For $m \leq M_{fs}$, the amplitude increase with distance which confirms the gradual recovery of the free space pattern as d increase. For $m < M_{fs}$ the amplitude decreases with d as a result of the energy being split over a higher number of modes.

The fitted and measured radiation patterns are compared in Fig. 8. Thus, as the results show, the model represents fairly well the general behaviour of perturbed antenna. The particular effects of the half space radiation and maximum and minimum radiation directions are well represented. A quantitative comparison of the error can be obtained in terms of the relative error $\epsilon(f)$ between the modelled and measured E-field defined as

$$\epsilon(f) = \frac{\|F_{\text{model}}(f,\theta,\phi) - F_{\text{meas}}(f,\theta,\phi)\|_2}{\|F_{\text{meas}}(f,\theta,\phi)\|_2}. \tag{11}$$

Fig. 9 report the relative error averaged over the measured frequencies. The total error is around $10\,\%$ for the co-polar and somewhat larger in the cross-polar direction. The Thomson antenna is radiating mainly over F_θ while F_ϕ value is very weak comparing to F_θ, thus F_ϕ error is higher than ϵ which is equivalent to F_θ error.

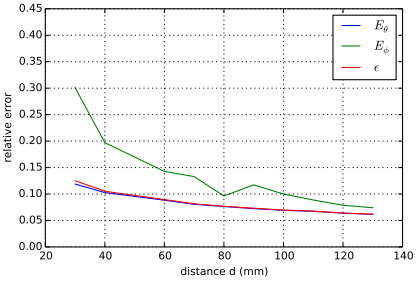

Fig. 9: Relative error (Thomson 1 antenna) averaged over the measured frequencies.

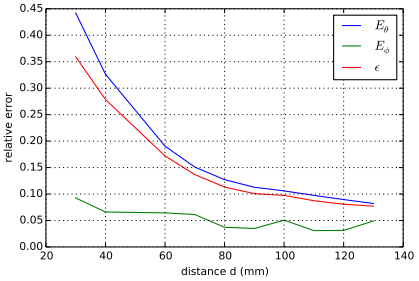

Fig. 11: Relative error (fractal antenna) averaged over the measured frequencies.

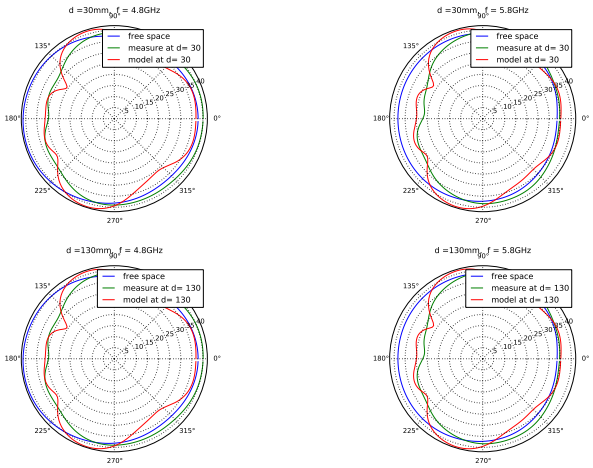

Fig. 10: Comparison of free-space, measured and modelled (fitted) radiation patterns in the (x,y)-plane for the Fractal antenna.

B. Model Validation

To validate the model, the same measurement campaign was carried out with a second antenna with a fractal structure depicted in Fig. 2. It appears from Fig. 10 that by using the model parameters in Table I obtained for the Thomson antenna, it is still possible to obtain a good prediction of the radiation pattern for the fractal antenna. The relative error in the fractal antenna is around $15\,\%$, Fig. 11. We observe higher relative error values at low distances and it might be due to measurement because antenna was not radiating as expected but for higher distances the results are equivalent to Thomson antenna results. We notice that fractal antenna, unlike Thomson antenna, is radiating similarly over F_θ and F_ϕ, therefore ϵ curve is between F_θ and F_ϕ curves.

VI. Conclusion

The simple spherical harmonic based model proposed in this paper allows to predict the perturbation of the free space antenna radiation pattern caused by the presence of a human phantom as a function of the antenna-phantom distance. The main purpose of the model is to obtain a fast access representation of the perturbed polarized antenna pattern for simulation of ultra wideband systems. This model can with relatively few parameters be advantageously integrated in a channel simulator where the body is approximated by dielectric cylinders. The dependency of the model parameters with dielectric cylinder dimension and constitutive parameters have still to be investigated. This work has demonstrated the following practical interesting fact that simple modification of the non perturbed antenna coefficient can reproduce reasonably accurate reconstruction of the antenna in the presence of a dielectric cylinder. In the future work, this model will be generalized and the different parameters should take into account the volume and the dimensions of the phantom.

Acknowledgment

This work has been carried out in the frame of the CORMORAN project, which is funded by the French National Research Agency (ANR) under the contract number ANR-11-INFR-010 and the framework of the ICT project ICT-248894 WHERE2, which is partly funded by the European Union.

References

[1] C. Roblin. Ultra compressed parametric modelling of uwb antenna measurements. In *Antennas and Propagation, 2006. EuCAP 2006. First European Conference on*, pages 1–8, 2006.

[2] R. Burghelea, S. Avrillon, and B. Uguen. Vector spherical harmonics antenna description for ir-uwb ray tracing simulator. In *Electromagnetics in Advanced Applications, 2009. ICEAA '09. International Conference on*, pages 303–306, 2009.

[3] R. Burghelea, S. Avrillon, and B. Uguen. Ultra-compact parametric modelling of three-dimensional antenna radiation pattern for impulse radio-ultra-wide band ray tracing. *Microwaves, Antennas Propagation, IET*, 6(11):1251–1258, 2012.

[4] J. Rahola, F. Belloni, and A. Richter. Modelling of radiation patterns using scalar spherical harmonics with vector coefficients. In *Antennas and Propagation, 2009. EuCAP 2009. 3rd European Conference on*, pages 3361–3365, 2009.

[5] E. Gueguen, F. Thudor, and P. Chambelin. A low cost uwb printed dipole antenna with high performance. In *Ultra-Wideband, 2005. ICU 2005. 2005 IEEE International Conference on*, pages 89–92, 2005.

[6] Troels Pedersen Marios Raspopoulos Ronald Raulefs Julien Stéphan Gerhard Steinboeck Bernard Uguen Wei Wang Yoann Corre, Mohamed Laaraiedh. Fp7 where2 deliverable d1.7 http://www.ict-where2.eu/documents/deliverables/deliverable-d1.7.pdf, July 2012.

[7] Yinchao Chen and T. Simpson. Radiation pattern analysis of arbitrary wire antennas using spherical mode expansions with vector coefficients. *Antennas and Propagation, IEEE Transactions on*, 39(12):1716–1721, 1991.

[8] J.E. Hansen and Institution of Electrical Engineers. *Spherical Near-field Antenna Measurements (p.17)*. IEE electromagnetic waves series.